TRANSACTIONS ON ELECTRICAL AND ELECTRONIC MATERIALS
Vol. 13, No. 4, pp. 171-176, August 25, 2012

Regular Paper

pISSN: 1229-7607 eISSN: 2092-7592
DOI: http://dx.doi.org/10.4313/TEEM.2012.13.4.171

Crystal Structure and Piezoelectric Properties of Four Component Langasite $A_3BGa_3Si_2O_{14}$ (A = Ca or Sr, B = Ta or Nb)

Hitoshi Ohsato†
BK21 Graduate School, Hoseo University, Asan 336-795, Korea, Department of Research. Nagoya Industrial Science Research Institute, Nagoya 464-0819, Japan, and Material Science and Engineering, Nagoya Institute of Technology, Nagoya 466-8555, Japan

Tsuyoshi Iwataki
Material Science and Engineering, Nagoya Institute of Technology, Nagoya 466-8555, Japan

Hiroki Morikoshi
Materials Research Center, TDK Co., Chiba 286-8588, Japan

Received April 13, 2012; Accepted June 19, 2012

As langasite $A_3BC_3D_2O_{14}$ compounds with piezoelectric properties exhibit no phase transition up to the melting point of 1,400-1,500℃, many high temperature applications are expected for the SAW filter, temperature sensor, pressure sensor, and so on, based on the digital transformation of wider bandwidth and higher-bit rates. It has a larger electromechanical coupling factor compared to quartz and also nearly the same temperature stability as quartz. The $La_3Ga_5SiO_{14}$ (LGS) crystal with the $Ca_3Ga_2Ge_4O_{14}$-type crystal structure was synthesized and the crystal structure was analyzed by Mill et al. It is also an important feature that the growth of the single crystal is easy. In the case of three-element compounds such as $[R_3]_A[Ga]_B[Ga_3]_C[GaSi]_DO_{14}$ (R=La, Pr and Nd), the piezoelectric constant increases with the ionic radius of R. In this study, crystal structures of four-element compounds such as $[A_3]_A[B]_B[Ga_3]_C[Si_2]_DO_{14}$ (A = Ca or Sr, B = Ta or Nb) are analyzed by a single crystal X-ray diffraction, and the mechanism and properties of the piezoelectricity depending on the species of cation was clarified based on the crystal structure.

Keywords: Four compound langasite $(Ca\ Sr)_3(La\ Nd)Ga_3Si_2O_{14}$, Crystal structure analysis by single crystals, Mechanism of piezoelectricity, Framework structure of langasite, High temperature performance

1. INTRODUCTION

Langasite $La_3Ga_5SiO_{14}$ (LGS) group crystals are now attracting researcher's attention on the properties of high temperature performance, because they exhibit no curie point and no phase transition up until a melting point of around 1,500℃ and also no pyroelectricity depending on the point group 32, which is the same as quartz [1]. The properties are applied to the direct measuring of the combustion (burning) pressure sensor at the high temperature and the high pressure in combusting engines [2]. The piezoelectric constant of langasite is a superior sensitivity characteristic k ~ 15-25 approximately 3 times that of quartz crystal k ~ 7% [1]. On the other hand, langasite has been expected for surface acoustic wave (SAW) filter, because of low loss (high Q) and near zero temperature coefficient of frequency (TCf).

† Author to whom all correspondence should be addressed:
E-mail: ohsato@naa.att.ne.jp

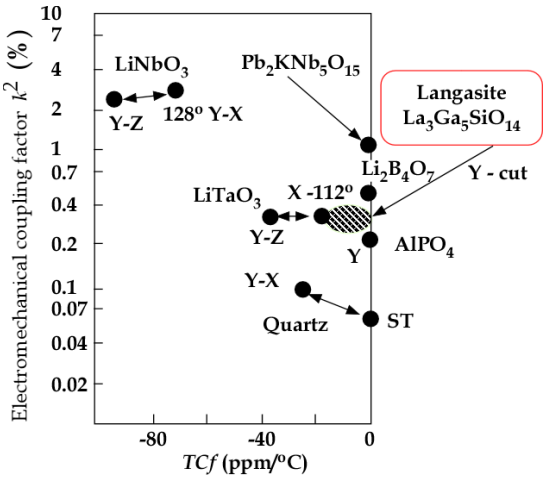

Fig. 1. Electromechanical coupling factor vs. temperature coefficient of frequency for piezoelectric materials.

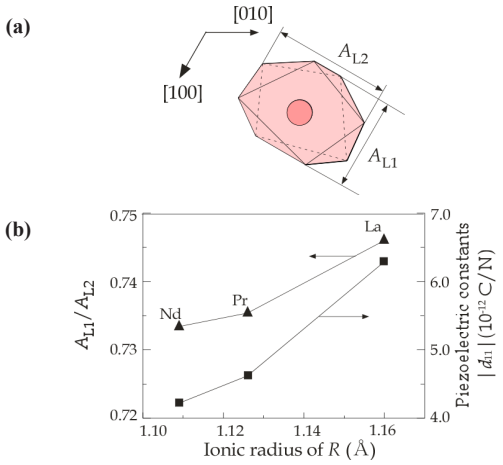

Fig. 3. (a) Size A_{L1} and A_{L2} of *A*-polyhedron along [100] and [120], respectively, (b) the ratio A_{L1}/A_{L2} and piezoelectric modulus $|d_{11}|$ as a function of the ionic radius of *R*.

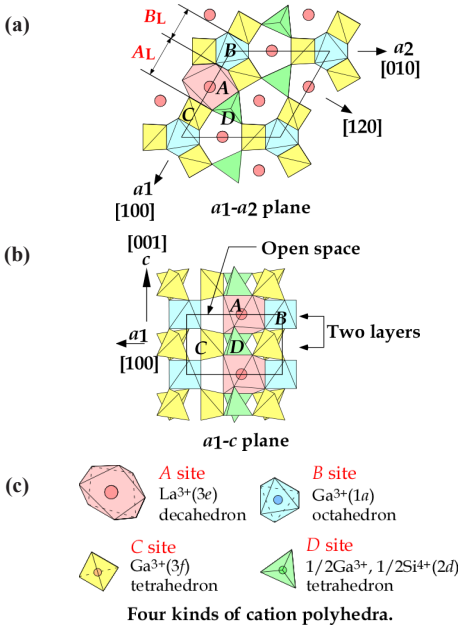

Fig. 2. Crystal structure of langasite. (a) and (b) are viewed from [001] and [120], respectively. (c) four kinds of cation polyhedra.

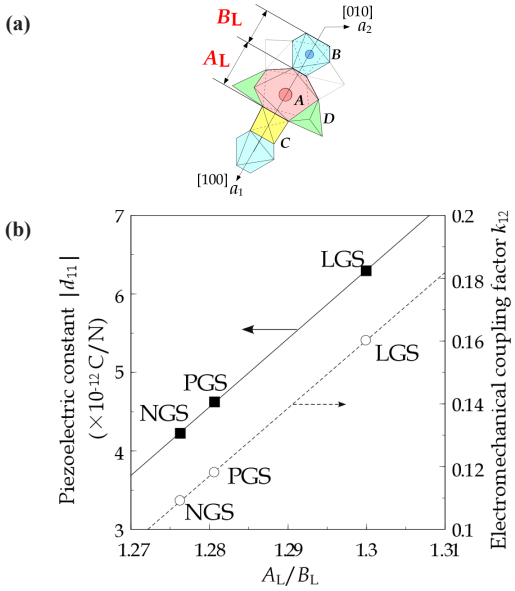

Fig. 4. (b) Piezoelectric constant d_{11}/electromechanical coupling factor k_{12} of LGS, PGS and NGS as a function of A_L/B_L which is shown in (a).

The *Q* values of LGS and $La_3Ga_{5.5}Nb_{0.5}O_{14}$ (LGN) are 30,000-40,000 and 60,000-120,000, respectively [1]. These values are higher than that of $LiTaO_3$ 5,000, but lower than that of quartz 100,000-200,000. Figure 1 shows the electromechanical coupling factor k^2 v.s. temperature coefficient of frequency regarding piezoelectric materials. Though some crystals are located around near zero *TCf*, $LiTaO_3$ crystal with wide-band does not show near zero *TCf* [1]. However, the $LiTaO_3$ SAW filter made by Yamaju Ceramics is used by roughly 60% of the world. Though $AlPO_4$ crystals with near zero *TCf* and a high electromechanical coupling factor K^2 are expected for SAW filter, they could not grow as good crystals because of twining during crystal growth. $Li_2B_4O_7$ crystal shows deliquescent and the growing speed is too slow. For langasite, the growing of crystals is easy and processing is superior because of their good properties, and langasite group compounds have fabricated more than 150 different compositions.

We presented three component compounds such as $R_3Ga_5SiO_{14}$ (*R* = La, Pr and Nd) [3-5], which are analyzed by single crystal X-ray diffraction. The crystal structure originally presented by Belokoneva et al. [6] and Mill et al. [7] is shown in Fig. 2. The structure has four oxygen polyhedra including cations: *A*-site of decahedron including La^{3+}, *B*-site of octahedron with Ga^{3+}, and two *C*-and *D*-sites of tetrahedra with Ga^{3+} and Si^{4+}. The crystal structural formulae are shown as $A_3BC_3D_2O_{14}$. These sites include many kinds of ions, which create compounds of more than 150 species.

Furthermore, the relationship between the deformation of decahedron (*A*-site) and piezoelectric modulus d_{11} was shown in Fig. 3 [8], and the piezoelectric constant d_{11} and the electromechanical coupling factor k_{12} are shown as a function of A_L/B_L as shown in Fig. 4. Also, we presented the mechanism of piezoelectric properties based on the crystal structure as shown in Fig. 5 [4,5,8]. The structure has an open-space on the row along the *a*-axis. It works as a buffer area and forms a net dipole moment according to moving the center of a mass regarding positive and negative charges, and produces dipole moments.

In this work, we investigated the crystal structures of four

component langasites: $Sr_3TaGa_3Si_2O_{14}$ (STGS), $Ca_3TaGa_3Si_2O_{14}$ (CTGS), $Sr_3NbGa_3Si_2O_{14}$ (SNGS), and $Ca_3NbGa_3Si_2O_{14}$ (CNGS) and clarified the effects for *A*-site substitution Sr for Ca on STGS/SNGS and CTGS/CNGS, and for *B*-site substitution Ta for Nb on STGS/CTGS and SNGS/CNGS. Moreover, we clarified the generation mechanism of the piezoelectricity and the reason why LGS has the best piezoelectric properties.

2. EXPERIMENTS

The crystals used for crystal structure analysis were grown by the Czochralski method. The conditions of the growth are shown in a previous paper [9]. A single crystal cut from the grown crystal was ground into a sphere and used for the single-crystal structure analysis. X-ray intensity data was obtained with Mo*Ka* radiation (λ=0.71069 Å) on a four-circle diffractometer using a graphite monochromator as shown in Table 1. After Lp and absorption correction, the refinement of the crystal structure was performed by the full-matrix least-squares program RADY [10]. The site occupancies for both *C*- and *D*-site Ga:Si were obtained from multiplicity *g* determined by the linear constraint as follows for *C*-site (position : 3*f*, multiplicity = 1/2) :

$$\begin{cases} g(Ga) = calc. \\ g(Si) = 1/2 - g(Ga) \end{cases}$$

and for *D*-site (position : 2*d*, multiplicity = 1/3) :

$$\begin{cases} g(Si) = calc. \\ g(Ga) = 1/3 - g(Si) \end{cases}$$

$B_{eq.}$ values were calculated from anisotropic temperature coefficients refined as follows:

$$B_{eq.} = 1/3 \sum_i \sum_j B_{ij} a^*_i a^*_j a_i . a_j .$$

The unit cell parameters were refined and determined by a least-square calculation of twenty values for 2θ between $70° \le 2\theta \le 80°$. The crystallographic data and experimental condition are shown in Table 2.

3. RESULTS AND DISCUSSION

The atomic coordinates of STGS, SNGS, CTGS, and CNGS are presented in Table 3(a) to (d), respectively. These crystal structures are converged successfully from 3 to 3.4 % for reliability factor *R* refining as a trigonal system and space group *P*321, as shown in Table 2. The lattice parameters of CTGS/CNGS are converged to *a* = 8.10 and *c* = 4.98 Å, and those of STGS/SNGS *a* = 8.29 and *c* = 5.08 Å. The lattice parameters of Sr-langasite are larger than Ca-langasite, because the ionic size of Sr (*r* = 1.26 Å) is larger than that of Ca (*r* = 1.12 Å). Those of Ta- and Nd-analogy are nearly the same, due to the similar ionic size of Ta and Nb ions (*r* = 0.64 Å). *C*- and *D*-sites are occupied mostly by Ga and Si, respectively, as shown in Table 3. The equivalent temperature factors $B_{eq.}$ of *B*-site (around 0.4 Å^2) and oxygen ions (around 0.9 Å^2) are reasonable values. Those of *A*-site (around 0.9 Å^2 for Ca-langasite and 0.6 for Sr-langasite) are a little large according to a large size polyhedron with a fluctuation of cations, and as the ionic size of Ca is small, the fluctuation becomes large. Further, *C*- and *D*-sites (around 0.5 Å^2) are also a little large because these sites are occupied by two cations Ga and Si. Especially, the *D*-site depends on the amount of site occupancies as shown in Fig. 6. Differences of oxygen positions (I, II, and III) on *A*-polyhedron

Table 1. Experimental conditions of STGS, SNGS, CTGS and CNGS.

	STGS	SNGS	CTGS	CNGS
Specimen radius (mm)	0.048	0.040	0.032	0.0047
Wave l ength of X-ray (Å)	0.71069	0.71069	0.71069	0.71069
Voltage (kV)	50	50	50	50
Current (mA)	200	200	250	200
Radius of collimator (mm)	0.5	0.5	0.5	0.5
Used monochromator	Graphite	Graphite	Graphite	Graphite
Bragg angle of monochromator	12.10	12.10	12.10	12.10
Scan mode	2θ-ω	2θ-ω	2θ-ω	2θ-ω
Scan speed (°/min)	8	8	16	16
Scan width (°)	1.155	1.313	1.207	1.523
Standard reflection #1	0 3 0	1 1 1	0 0 2	0 2 1
#2	0 2 0	0 2 1	-1 -1 1	1 2 1
#3	0 2 -1	-1 2 1	0 -2 1	1 1 1
Range of 2θ	120	120	120	120
No. of measured reflections	3,499	3,479	3,295	3,285
No. of used reflections	3,075	2,451	2,835	2,701
No. of refined parameters	45	45	45	45

Table 2. Cyrstal data of STGS, SNGS, CTGS and CNGS.

	STGS	SNGS	CTGS	CNGS
Formula weight	933.138	845.096	790.518	702.476
Crystal system	trigonal	trigonal	trigonal	trigonal
Space group	*P*321	*P*321	*P*321	*P*321
Point group	32	32	32	32
Lattice parameter *a* (Å)	8.2926(4)	8.2843(5)	8.1098(5)	8.0947(6)
c (Å)	5.0775(8)	5.0772(10)	4.9833(6)	4.9822(8)
Unit cell volume (Å^3)	302.38(5)	301.76(6)	283.83(5)	282.72(5)
Formula number *Z*	1	1	1	1
Calculated density D_x (g/cm^3)	5.1244	4.6505	4.6249	4.1261
Linear absorption coefficient μ (cm^{-1})	304.562	218.940	191.244	99.939
R	0.0300	0.0344	0.0339	0.0308
R_W	0.0254	0.0261	0.0308	0.0270
GOF	1.2979	1.2246	1.1110	1.3828

Table 3. Atomic coordinates and anisotropic temperature factor of STGS (a), SNGS (b), CTGS (c), and CNGS (d).

(a) Atomic parameter of STGS($[Sr_3]_A[Ta]_B[Ga_3]_C[Si_2]_DO_{14}$)

atom	site	occupancy	*x*	*y*	*z*	$B_{eq.}$
Sr	3*e*	1	0.42896(5)	0	0	0.633(5)
Ta	1*a*	1	0	0	0	0.384(2)
Ga1	3*f*	1.00(1)	0.74640(5)	0	1/2	0.486(6)
Si1		0.0				
Si2	2*d*	0.972(3)	1/3	2/3	0.4648(2)	0.54(1)
Ga2		0.028				
O1	2*d*	1	1/3	2/3	0.7765(6)	0.86(3)
O2	6*g*	1	0.4745(3)	0.3071(3)	0.6660(4)	0.87(4)
O3	6*g*	1	0.2213(3)	0.0948(4)	0.2313(4)	0.77(4)

Anisotropic temperature factor of STGS

atom	β_{11}	β_{22}	β_{33}	β_{12}	β_{13}	β_{23}
Sr	0.00296(1)	0.00343(2)	0.00595(7)	1/2*β_{22}	0.00002(3)	2*β_{13}
Ta	0.002039(6)	β_{11}	0.00301(4)	1/2*β_{11}	0	0
Ga, Si	0.00241(1)	0.00247(2)	0.00442(8)	1/2*β_{22}	0.00029(3)	2*β_{13}
Si, Ga	0.00263(4)	β_{11}	0.0053(2)	1/2*β_{11}	0	0
O1	0.00464(9)	β_{11}	0.0066(5)	1/2*β_{11}	0	0
O2	0.00293(8)	0.0064(1)	0.0075(4)	0.0026598)	-0.0010(2)	-0.0025(2)
O3	0.00325(8)	0.0044(1)	0.0079(3)	0.00225(7)	-0.0015(1)	-0.0031(2)

(b) Atomic parameter of SNGS($[Sr_3]_A[Nb]_B[Ga_3]_C[Si_2]_DO_{14}$)

atom	site	occupancy	x	y	z	$B_{eq.}$
Sr	3*e*	1	0.42890(4)	0	0	0.592(5)
Nb	1*a*	1	0	0	0	0.433(5)
Ga1	3*f*	0.99(1)	0.74699(5)	0	1/2	0.454(5)
Si1		0.01				
Si2	2*d*	0.933(3)	1/3	2/3	0.4647(2)	0.45(1)
Ga2		0.007				
O1	2*d*	1	1/3	2/3	0.7789(6)	0.78(3)
O2	6*g*	1	0.4743(3)	0.3073(3)	0.6666(4)	0.80(4)
O3	6*g*	1	0.2197(2)	0.0931(3)	0.2315(3)	0.78(4)

Anisotropic temperature factor of SNGS

atom	β_{11}	β_{22}	β_{33}	β_{12}	β_{13}	β_{23}
Sr	0.00287(1)	0.00322(2)	0.00529(6)	1/2*β_{22}	0.00010(3)	2*β_{13}
Nb	0.00229(2)	β_{11}	0.0034(1)	1/2*β_{11}	0	0
Ga, Si	0.00230(1)	0.00231(2)	0.00400(7)	1/2*β_{22}	0.00034(3)	2*β_{13}
Si, Ga	0.00212(4)	β_{11}	0.0045(2)	1/2*β_{11}	0	0
O1	0.0046(1)	β_{11}	0.0043(5)	1/2*β_{11}	0	0
O2	0.00236(9)	0.0056(1)	0.0072(4)	0.00185(9)	-0.0010(1)	-0.0022(2)
O3	0.00359(9)	0.0046(1)	0.0076(4)	0.00257(8)	-0.0015(2)	-0.0028(2)

(c) Atomic parameter of CTGS($[Ca_3]_A[Ta]_B[Ga_3]_C[Si_2]_DO_{14}$)

atom	site	occupancy	x	y	z	$B_{eq.}$
Ca	3*e*	1	0.4242(1)	0	0	0.91(1)
Ta	1*a*	1	0	0	0	0.384(2)
Ga1	3*f*	0.99(1)	0.74525(2)	0	1/2	0.511(6)
Si1		0.01				
Si2	2*d*	0.987(3)	1/3	2/3	0.5503(2)	0.53(1)
Ga2		0.013				
O1	2*d*	1	1/3	2/3	0.2297(6)	0.987(3)
O2	6*g*	1	0.4763(3)	0.3194(3)	0.3111(4)	0.89(4)
O3	6*g*	1	0.2242(3)	0.0851(3)	0.7643(4)	0.76(4)

Anisotropic temperature factor of CTGS

atom	β_{11}	β_{22}	β_{33}	β_{12}	β_{13}	β_{23}
Ca	0.00416(3)	0.00740(5)	0.0068(2)	1/2*β_{22}	-0.00063(7)	2*β_{13}
Ta	0.002154(7)	β_{11}	0.00305(4)	1/2*β_{11}	0	0
Ga, Si	0.00273(2)	0.00278(2)	0.00405(9)	1/2*β_{22}	-0.00025(3)	2*β_{13}
Si, Ga	0.00279(4)	β_{11}	0.0049(2)	1/2*β_{11}	0	0
O1	0.0060(1)	β_{11}	0.0055(5)	1/2*β_{11}	0	0
O2	0.00290(9)	0.0063(1)	0.0088(4)	0.00237(9)	0.0013(2)	0.0034(2)
O3	0.0040(1)	0.0048(1)	0.0074(4)	0.00288(8)	0.0019(2)	0.0024(2)

(d) Atomic parameter of CNGS($[Ca_3]_A[Nb]_B[Ga_3][Si_2]_DO_{14}$)

atom	site	occupancy	x	y	z	$B_{eq.}$
Ca	3*e*	1	0.42424(6)	0	0	0.854(8)
Nb	1*a*	1	0	0	0	0.439(3)
Ga1	3*f*	1	0.74640(3)	0	1/2	0.493(3)
Si1		0				
Si2	2*d*	0.989(2)	1/3	2/3	0.5505(2)	0.490(8)
Ga2		0.011				
O1	2*d*	1	1/3	2/3	0.2321(5)	0.96(2)
O2	6*g*	1	0.4766(2)	0.3209(2)	0.3130(3)	0.84(3)
O3	6*g*	1	0.2232(2)	0.0833(2)	0.7637(3)	0.74(3)

Anisotropic temperature factor of CNGS

atom	β_{11}	β_{22}	β_{33}	β_{12}	β_{13}	β_{23}
Ca	0.00393(2)	0.0690(3)	0.00635(9)	1/2*β_{22}	-0.00065(5)	2*β_{13}
Nb	0.00246(1)	β_{11}	0.00351(6)	1/2*β_{11}	0	0
Ga, Si	0.002600(9)	0.00268(1)	0.00450(4)	1/2*β_{22}	-0.00031(2)	2*β_{13}
Si, Ga	0.00261(3)	β_{11}	0.0045(2)	1/2*β_{11}	0	0
O1	0.00589(8)	β_{11}	0.0056(2)	1/2*β_{11}	0	0
O2	0.00320(6)	0.00630(9)	0.0077(3)	0.00276(6)	0.0010(1)	0.0028(1)
O3	0.00338(6)	0.00457(7)	0.0076(3)	0.00240(6)	0.0014(1)	0.0026(1)

in regards to four component langasites are shown in Fig. 7. We brought out two effects for substitutions of *A*- and *B*-cations. The first one is *A*-site substitution Sr for Ca on STGS/SNGS and CTGS/CNGS. The second one is *B*-site substitution Ta for Nb on

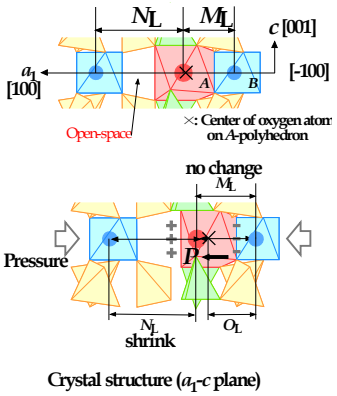

Fig. 5. Origin of piezoelectricity on langasite projected from [120]. Position X is the center of oxygen atoms on *A*-polyhedron. Under pressure, M_L does not change and N_L shrinks because of the role of open-space as a damper.

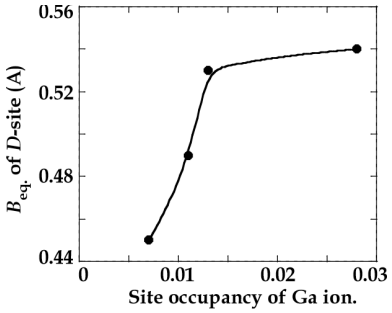

Fig. 6. The equivalent temperature factor $B_{eq.}$ of *D*-site as a function of site occupancy for Ga ion.

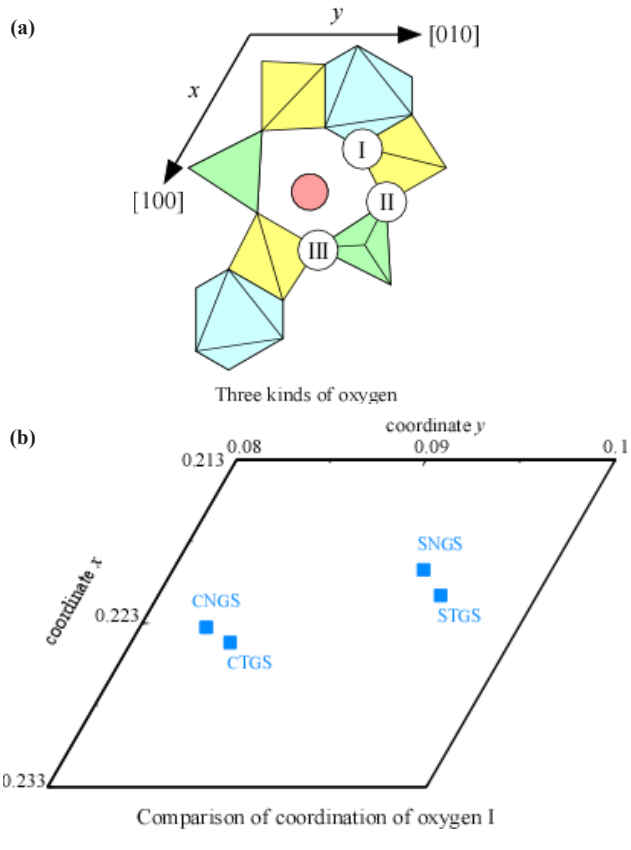

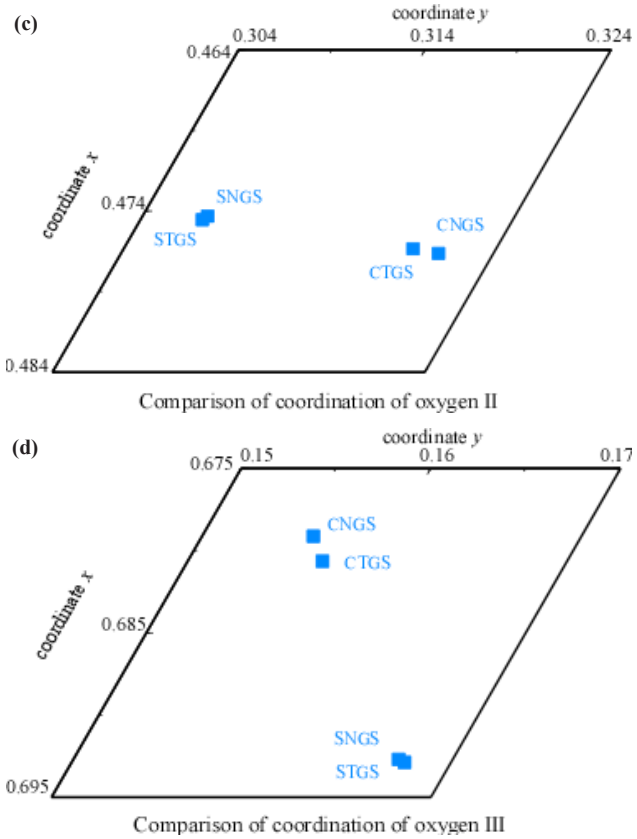

Fig. 7. The coordinates of three oxygen ions I (b), II (c), and III (d) on STGS, SNGS, CTGS, and CNGS crystals.

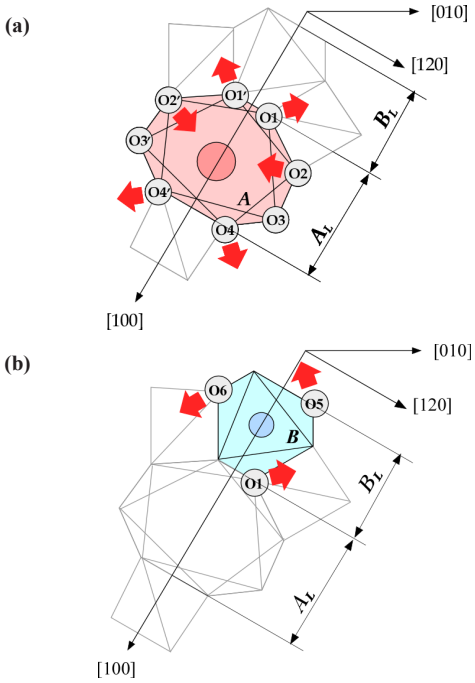

Fig. 8. (a) Deformation of *A*-polyhedron by substitution Sr for Ca. As a result, *A*-polyhedron expands toward [100] and shrinks toward [120], (b) deformation of *B*-polyhedron by substitution Ta for Nd. The equivalent oxygen ions rotate around the 3-fold axis, and the B_L length becomes large.

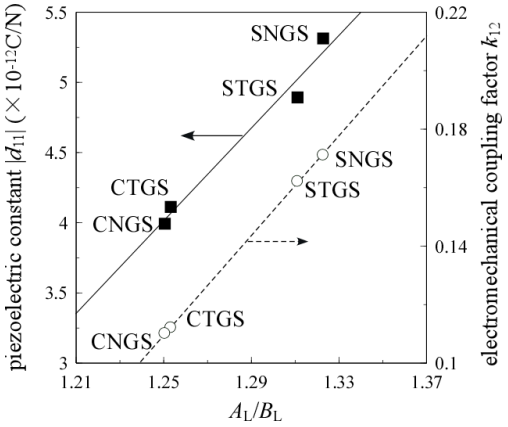

Fig. 9. Piezoelectric constant d_{11}/electromechanical coupling factor k_{12} of STGS, SNGS, CTGS, and CNGS crystals as a function of A_L/B_L, which is shown in Fig. 4(a).

STGS/CTGS and SNGS/CNGS. In the case of the first one, shifts of oxygen ions are large: oxygen I and III shift towards expanding, and oxygen II shift towards shrinking, as shown in Fig. 8(a). As a result, *A*-polyhedron expands toward [100] and shrinks toward [120]. In the case of the second one, shifts of oxygen ions in *B*-octahedron are small as seen in Fig. 7, because the ionic size difference between Nb and Ta is small. The oxygen ions being equivalent rotate around the 3-fold axis as shown in Fig. 8(b). As a result, B_L becomes large and A_L does not change. The ionic radius of Ta is empirically larger than that of Nd. We present the piezoelectric constant d_{11} and the electromechanical coupling factor k_{12} of 4-component langasites as a function of A_L/B_L as shown in Fig. 9. Expansion toward [100] obtained in the case of *A*-site substitution by a large ion brings about large value regarding A_L/B_L. So, Sr-substituted langasites have large d_{11} and k_{12}. In the case of *B*-site substitution, as A_L does not change, the property differences between Nb and Ta are not significant.

4. CONCLUSIONS

Four component langasite STGS, SNGS, CTGS, and CNGS crystal structures are analyzed by X-ray single crystal structure analysis. The crystal data such as trigonal, *P*321, lattice constants, as well as the atomic parameters and anisotropic temperature coefficients for each cation are presented by precise analysis of the reliability factor *R* of approximately 3%. The values for d_{11} and k_{12} are presented as a function of the A_L/B_L ratio, which show a complete linear relationship. Two effects for substitutions *A*- and *B*-site cations are presented: the substitution Sr for Ca brings expansion toward [100] and an increase of A_L/B_L enlarges d_{11} and k_{12}. On the other hand, as the substitution Ta for Nb brings little change, the property values are similar.

ACKNOWLEDGMENTS

The author would like to thank to Dr. K. Kawasaki and Dr. J. Sato of TDK Co. for the presenting of single crystals. Also, Professors Cheon Chae-Il and Kim Jeong-Seog of Hoseo University for discussion of the contents, and Professors Ken-ichi Kakimoto and Isao Kagomiya of NIT for supporting experimental conditions. A part of this presentation was supported by A Grant-in Aid for Science Research (C) from the Ministry of Education, Science, Sports and Culture, Japan.

REFERENCES

[1] T. Fukuda, K. Shimamura, T. Kohno, H. Takeda, and M. Sato, J. Jap. Asso. Crystal Growth, **22**(5), 358 (1995).
[2] K. Tsukada, M. Takeuchi, S. Tokumitsu, Y. Ohmura, and K. Kawaguchi, R&D Review of Toyota CRDL, **28**(4), 49 (1993).
[3] T. Iwataki, H. Ohsato, K. Tanaka, H. Morikoshi, J. Sato, and K. Kawasaki, J. Eur. Ceram. Soc., **21**, 1409 (2001) [DOI: 10.1016/S0955-2219(01)00029-2].
[4] H. Ohsato, *Materials Science and Technology*, ISBN 978-953-51-0193-2, edited by S. D. Hutagalung, (Intech, Rijeka, Croatia, 2012) Chapter 2.
[5] H. Ohsato, T. Iwataki, and H. Morikoshi, Trans. Electr. Electron. Mater., **13**(2), 51 (2012) [DOI: 10.4313/TEEM.2012.13.2.51].
[6] E. L. Belokoneva, M. Simonov, A. V. Butashin, B. V. Mill, and N. V. Belov, Sov. Phys. Dokl., **25**, 954 (1980).
[7] B. V. Mill, A. V. Buntashin, G. G. Khodzhabagyan, E. L. Belokoneba, and N. V. Belov, Dokl. Akad. Nauk USSR, **264**, 1385 (1982).
[8] N. Araki, H. Ohsato, K. Kakimoto, T. Kuribayashi, Y. Kudoh, and H. Morikoshi, J. Eur. Ceram. Soc., 27, 4099 (2007) [DOI: 10.1016/j.jeurceramsoc.2007.02.177].
[9] J. Sato, H. Takeda, H. Morikoshi, K. Shimamura, P. Rudolph, and T. Fukuda, J. Crystal Growth, **191**, 746 (1998) [DOI: 10.1016/S0022-0248(98)00362-5].
[10] S. Sasaki, XL Report, ESS, State Univ. of New York, pp.1, (1982).